COUPLING AND DECOUPLING OF HEAT AND HELIUM TRANSPORT
IN A GEOTHERMAL RESERVOIR

Judith L. Andrews[1] and Martin O. Saar[2]

University of Minnesota – Twin Cities
Department of Geology & Geophysics
Minneapolis, MN, 55455, U.S.A.
e-mail: [1]andre345@umn.edu [2]saar@umn.edu

ABSTRACT

We present two- and three-dimensional simulations of heat and helium transport for a generalized graben system to systematically investigate how various interacting parameters influence coupling and decoupling of magmatic or mantle heat and helium signals in the Earth's crust. We confirm findings of previous studies by other authors including the occurrence of spatial decoupling of heat and helium due to variations in their respective diffusivities, entrapment of helium by low permeability layers, and the preference of helium for fracture flow. We continue by assessing the impact of radiogenic heat and helium production and buoyancy-driven convection within a fracture system and within a crystalline basement layer on the distribution of temperature, helium, and isotopic helium ratios. We find that processes deep within the subsurface can have a large effect on near-surface mantle/magmatic heat and helium signatures even though such near-surface measurements are typically used to infer deep groundwater and heat flow vector fields. Additionally, we show the significance of distinguishing between heat and helium signal decoupling due to transport phenomena and due to other subsurface processes. The results of our investigation have applications to geothermal reservoir analyses, mantle heat versus mantle helium estimations, and studies using heat and/or helium as natural tracers of groundwater flow.

1. INTRODUCTION

Heat and helium are often used as natural tracers in groundwater flow systems. In geothermal reservoirs and volcanic regions, geoscientists typically utilize heat and helium from the mantle and magmas to evaluate geothermal resources or to constrain the size of volcanic plumbing systems. As a result, there is a considerable amount of published research concerning investigations of heat and variations in helium isotope concentrations in these regimes. However, the interdependence of various aquifer properties and their effect on the near-surface signals of heat and helium remain poorly constrained.

While there is little doubt that the patterns of coupling and decoupling carry important information about the groundwater flow regime, difficulties arise in understanding how the various parameters affecting the transport and strength of these signals interact. For example, decoupling is due in part to the varied diffusivities of heat and helium. Helium has a lower diffusivity than heat and will thus show significant advective transport at lower fluid velocities (Bickle & McKenzie, 1987). Additionally, helium is prone to entrapment by low permeability layers, and often relies on seismic activity to create and maintain permeable conduits for transport. Moreover, radiogenic production of ^{4}He due to the decay of uranium (^{235,238}U) and thorium (^{232}Th) in the Earth's crust can lower the ratio of ^{3}He to ^{4}He, thereby diluting the magmatic or mantle ^{3}He signal while also generating heat.

Because magmatic intrusions and the mantle provide both heat and helium to the Earth's crust, a first-order assumption is that near-surface heat and helium signals should be coupled. However, in seismically active regions, such as the Rhine Graben in southwestern Germany, temperature and magmatic helium anomalies are often spatially and/or temporally decoupled near the Earth's surface (Clauser et al., 2002).

There is abundant information available about the influence of aquifer characteristics on the transport of heat, for example, Bredehoeft & Papadopulos (1965), Smith & Chapman (1983), Clauser & Villinger (1990), Lopez & Smith (1995), Clauser et al. (2002), Bächler et al. (2003), and Saar & Manga (2004). Investigations of how physical and subsurface parameters impact heat and helium transport are commonly case studies, for example, those by Stute et al. (1992), Torgersen et al. (1994), Torgersen et al. (1995), Zhao et al. (1998), Castro et al. (1998b), Castro et al. (2005), and Saar et al. (2005). Generalized, one-dimensional quantitative analyses of heat and helium transport include Bickle & McKenzie (1987), Torgersen (1993), and Bach et al. (1999). It appears, however, that there are no systematic two- and three-dimensional simulations investigating the effects of aquifer, heat, and helium characteristics to show how these parameters interact and affect the resulting near-surface expressions.

In this contribution, we investigate the effects of the following on interpretation of near-surface heat and helium signals: 1) permeability variations within the system, 2) buoyancy-driven convection in a

fracture and in a crystalline basement, and 3) radiogenic heat and helium production in a basement. We find that not only do permeabilities determine temperature and helium patterns, but that buoyancy-driven convection and radiogenic heat and helium production—even at great depth—can also have large effects on the spatial and temporal distribution of heat and helium signals observed near the surface.

2. BACKGROUND & CONCEPTUAL MODEL

Because helium is inert, it is an excellent tracer of groundwater flow. It does not adsorb onto mineral surfaces and takes no part in chemical reactions. Further, each source of helium has a unique isotopic signature. Atmospheric helium has an average isotopic ratio of $[^3He]_a/[^4He]_a = 1R_a \approx 1.4 \times 10^{-6}$ (O'Nions & Oxburgh, 1983). High magmatic or mantle ratios are typically found at mid-ocean ridges, with values of $R_m = [^3He]_m/[^4He]_m \approx 8R_a$ (Oxburgh & O'Nions, 1987). Due to in-situ radiogenic production of ^4He, crustal helium exhibits a much lower ratio on the order of $R_c = [^3He]_c/[^4He]_c \approx 0.02R_a$ (Ozima & Podosek, 2002). When relative contributions of heat and helium sources are constrained, they can provide information, difficult to obtain by other means, such as insight into deep crustal groundwater flow processes and circulation systems in which residence times are too large for the use of ^{14}C dating (Stute et al., 1992) and anthropogenic tracer analyses.

Our model (Figure 1) is adapted from Lopez & Smith (1995). In their heat and groundwater flow study, they find the limits in permeability space that control whether heat transport in a fracture is controlled by conduction, advection (topography-driven convection), or buoyancy-driven convection.
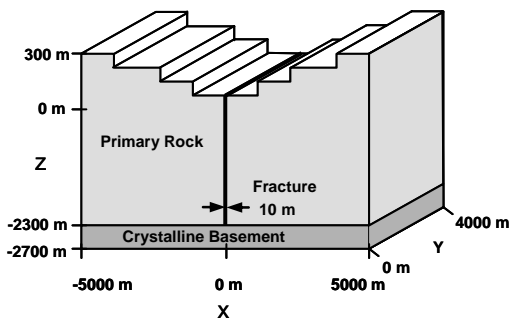

Figure 1. Diagram of three-dimensional model domain. The two-dimensional model that is also used is a 100-m thick slice of the three-dimensional version, with orientation perpendicular to the fracture.

Heat and mass transport is modeled for a symmetric aquifer containing three materials representing crystalline basement, fracture, and primary (country) rock (Figure 1). At the base of the

model is a 400m-thick layer representing the uppermost portion of the crystalline basement. A vertical mid-basin fracture (located at x=0m) system extends to the top of the basement and is modeled as a 10m-wide zone of high permeability. The rest of the model is comprised of a primary rock material that could represent all orders of potential fill, such as sandstone and limestone. Permeabilities of the primary rock, fracture, and basement vary according to the desired transport regime (Table 1). We assume that each unit is isotropic and homogeneous such that the second-rank permeability tensor, **k**, can be simplified to a scalar value, k.

Table 1. Permeabilities (m^2) for various thermal transport regimes, as given by Lopez & Smith (1995).

[1]*Sections 3.1.1, 3.3.1* [2]*Section 3.1.2* [3]*Section 3.2* [4]*Section 3.3.2*

	Host Rock	Fracture	Basement
Advective[1]	4×10^{-16}	1×10^{-13}	1×10^{-22}
Diffusive[2]	1×10^{-19}	1×10^{-16}	1×10^{-22}
Buoyant Convection in Fracture[3]	4×10^{-16}	1×10^{-12}	1×10^{-22}
Buoyant Convection in Basement[4]	4×10^{-16}	1×10^{-13}	4×10^{-16}

Topography-driven (advective) flow is initiated by an average slope of 300m/5km along the shoulders of the basin. There is no variation in slope along the y-direction. Because our study concentrates on processes over a depth of three kilometers, we ignore unsaturated flow between the surface and the water table.

Consistent with the model from Lopez & Smith (1995), the following parameters apply: thermal conductivity for all materials is 2.5W/m·°C, basal heat flux is 90mW/m², the pore fraction of the primary rock, fracture, and basement are 0.10, 0.50, and 0.01, respectively. Surface boundary conditions are a uniform temperature of 10°C and a constant pressure of 1×10^5Pa. Thus, due to the small relief considered, we ignore the small effects of an adiabatic lapse rate. Additionally, we apply a surface boundary condition for helium, with helium concentrations for air saturated water (neglecting excess air helium from solution of bubbles that are entrapped during groundwater table fluctuations) at 10°C of $[^3He] \approx 6 \times 10^{-14}$ and $[^4He] \approx 5 \times 10^{-8}$ cm³/g(H₂O)STP.

As described in Lopez & Smith (1995), model dimensions are $-5000 \leq x \leq 5000$m, $-2700m \leq z \leq 300m$ and $0 \leq y \leq 4000m$ (for three-dimensional simulations). Grid spacing in y and z remains constant at 100m, while grid spacing along x (perpendicular to the fracture system) is irregular,

allowing for greater resolution near the fracture. In our two- and three-dimensional models, the number of cells is 541 and 21,160, respectively.

We use the EOSN module (Shan & Pruess, 2003) of TOUGH2 (Pruess et al., 1999) to model diffusive and advective flow of heat, helium, and water. Models are brought to steady-state before the inclusion of source terms. We include source terms for basal heat and helium flux in the cells of the bottom-most layer. Helium diffusivity is the EOSN default value of $10^{-9} m^2/s$ (Shan & Pruess, 2003).

To estimate the basal helium flux, we first assume a MORB-similar mantle or magmatic intrusion with $R=8R_a$ (Oxburgh & O'Nions, 1987). We then consider transport of the gases through several kilometers of crystalline basement, causing accumulation of additional ^4He, thus lowering R (Hilton, 1996). Using a mantle helium flux of $2 \times 10^9 atoms/m^2 s$ (Oxburgh & O'Nions, 1987) as a basis, then adding sufficient ^4He to decrease R to $6R_a$, results in fluxes of ^3He and ^4He of $1.0 \times 10^{-22} kg/m^2 s$ and $1.6 \times 10^{-17} kg/m^2 s$, respectively. Magmatic heat and helium flux at the base of the model remain constant for all simulations. In each case, maximum temperatures for steady-state conditions are approximately 110°C. Due to the pressure field, no boiling occurs in the model. Helium concentrations within the fracture and primary rock vary, but remain consistent with published values, reaching up to $10^{-3} cm^3/g(H_2O)STP$ (Griesshaber et al, 1992; Castro et al., 2005).

3. DISCUSSION OF SIMULATION RESULTS

In this section, we describe the results of changing the permeability of the fracture zone and primary rock that create coupled and decoupled transport of heat and helium (Section 3.1), the effect of buoyancy-driven convection within a fracture (Section 3.2), radiogenic heat and helium production in the basement (Section 3.3.1), and the combined effect of radiogenic processes and buoyancy-driven convection in the crystalline basement (Section 3.3.2).

For ease of comparison, we reduce all variables to dimensionless values. Ratios of $R=[^3He]/[^4He]$ are normalized by the atmospheric ratio, R_a. Helium concentrations and temperature are reported as fractions of the maximum value in the model, such that $[He]_o=[He]/[He]_{max}$, where $[He]=[^3He]+[^4He]$, and $T_o=T/T_{max}$.

3.1 Permeability

3.1.1 Coupled Advective Transport

Typically, permeabilities $\geq 10^{-17} m^2$ are sufficiently high to allow for advective transfer of both heat and helium (Manning & Ingebritsen, 1999), so that the two signatures remain coupled (Figure 2).

Patterns of both signals are determined by the direction of flow, with the lowest temperatures and helium concentrations in recharge areas. The discharge zone near the fracture exhibits the highest temperatures and concentrations of helium (Figures 2 and 6a). Also note the difference in the widths of the increased signals in the primary rock layer (Figure 2a). The sharper helium peak in the fracture is a result of the greater influence of advection on helium transport than on heat transport. This pattern is seen in each simulation.
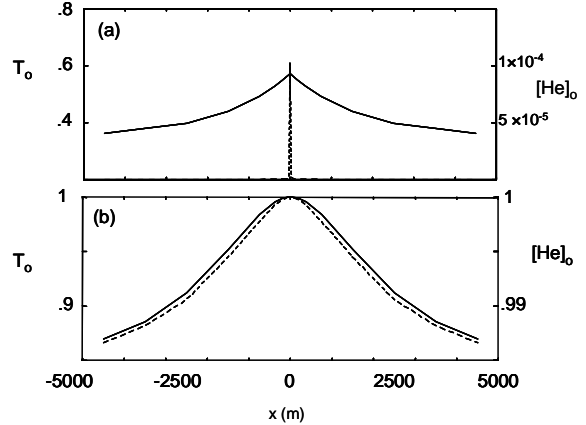

Figure 2.   Temperature and helium signals for the coupled advective transport simulation: (solid lines) T_o, (dashed lines) $[He]_o$ Maximum values of temperature and [He] coincide at the fracture. (a) y=50m, z = -1050m: primary (host) rock (b) y=50m, z = -2650m: basement layer

3.1.2 Decoupled Transport

Heat and helium have contrasting diffusivities, and therefore also have different permeability thresholds above which transport becomes advectively controlled. For heat, the lower threshold is on the order of $10^{-17} m^2$, whereas for helium the threshold is approximately $10^{-20} m^2$. Between the two threshold values is a range in which transport of heat is controlled by diffusion but helium transport is controlled by advection (Manning & Ingebritsen, 1999).

The result of mixed transport processes for heat and helium is a decoupling of the two signals. Thus, at a given elevation, higher temperatures occur under topographic highs (recharge areas) whereas higher mantle/magmatic helium concentrations occur at topographic lows (discharge areas) (Figure 3). Temperature contours mimic the overlying topography, as typical for diffusion-dominated systems, while helium concentration contours are oppositely shaped, indicating the direction of fluid transport and related helium advection.
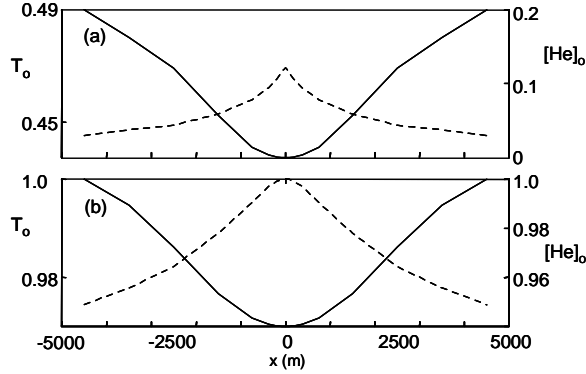
Figure 3. Decoupled Transport: (solid lines) T_o, (dashed lines) $[He]_o$ Maximum values of temperature and [He] do not coincide, helium exhibits high values at the fracture, while temperature is highest along the sides of the model. (a) y=50m, z= -1050m: host rock (b) y=50m, z= -2650m: basement layer.

3.2 Buoyancy-Driven Fracture Convection

When fracture permeability is high and there is sufficient heat flow at the base of the system, buoyancy-driven convection cells form inside the fracture (Figure 4). Buoyancy-driven fracture convection is effective at bringing surface waters to great depth, creating a well-mixed system.
Because fluids within the fracture are well-mixed, helium ratios remain relatively consistent throughout. Due to the continued influx of heat and helium from the base of the model, high concentrations and temperatures are still observed at discharge zones.
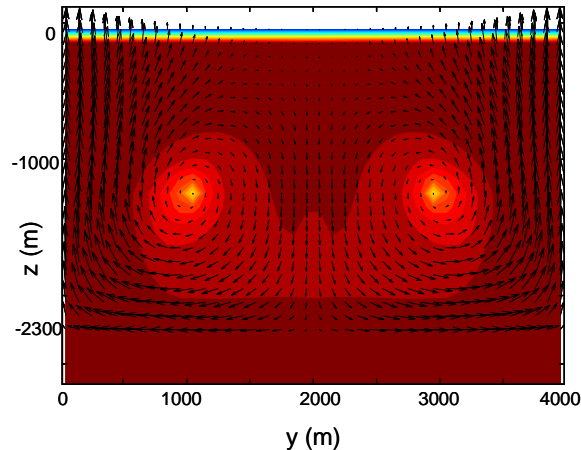

Figure 4. Distribution of R/R_a values in the fracture for the case of buoyancy driven convection. Arrows represent relative velocity of fluid flow. Color contours represent values of R/R_a, the deep red represents high values of ~$6R_a$, blue represents atmospheric values. See Figure 7 for complete color scale.

3.2.1 Temperature

Temperatures exhibit little lateral variation throughout the basement and primary rock (Figure 7b, right column). For systems in which buoyancy-driven convection occurs in a fracture, heat flow in the primary (country) rock is chiefly through conduction (Lopez & Smith, 1995; Clauser et al., 2002).

In the fracture, the temperature signal clearly reflects zones of upwelling and downwelling. In Figure 5a-i, the sharp decrease in temperature at the fracture indicates mixing with colder surface water (downwelling). In Figure 5b-i, temperatures increase rapidly near the fracture, indicating that fluids are advecting heat from the basement up toward the surface (upwelling). Figure 6b-ii also shows this variation in temperature at discharge and recharge zones.

3.2.2 Helium Concentration

Helium concentrations are extremely low throughout much of the basin, in both the primary rock and the fracture. Exceptions are the two zones of upwelling at y≈50m, y≈3950m (Figure 6b-i). Although helium concentrations at recharge zones approach the concentration of air saturated water, values of R/R_a remain consistent with that of the basal helium flux, $R=6R_a$ (Figure 4).
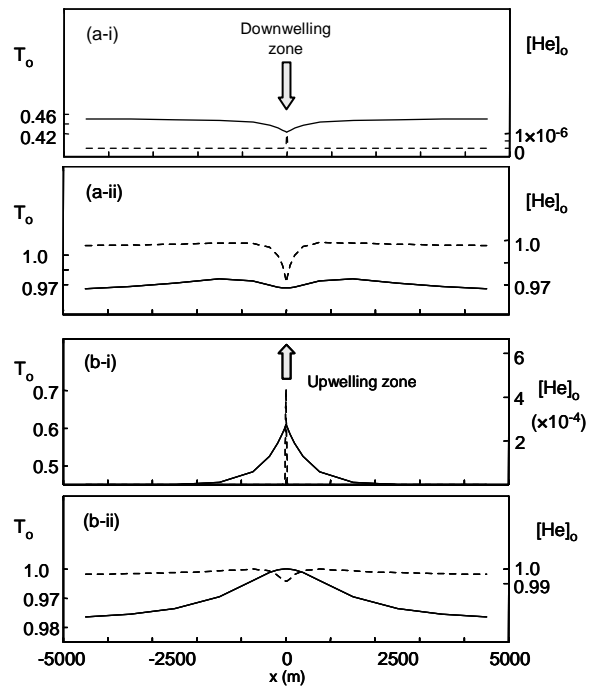

Figure 5. Temperature and helium signals for the buoyancy-driven fracture convection model: (solid lines) T_o, (dashed lines) $[He]_o$. (a) y= 2000m: recharge zone. (b) y= 50m: discharge zone. (i) z= -1050m: primary rock layer. (ii) z= -2650m: basement layer.

There are three interesting effects of buoyancy-driven fracture convection on heat and helium signals, taken from three different perspectives:

1. In the fracture (y-z view, Figure 4): temperature and helium concentrations are low except in discharge areas, while R/R_a values remain elevated throughout.

2. In the primary rock (x-z view, Figure 7b): R/R_a and helium concentrations are low, while temperature is elevated.

3. In the primary rock near the fracture (x-y view, Figure 6b): helium concentrations and temperature are low everywhere except discharge areas. R/R_a is elevated at discharge and recharge areas.

3.3 Radiogenic Processes

To show the effect of radiogenic heat and helium production on R values, we add source terms to the crystalline basement layer, in Section 3.3.1. We assume heat production of $3\mu W/m^3$, typical for granite and gneiss basements (Clauser & Villinger, 1990; Castro et al, 1998a). Production of ^{4}He is estimated using the ratio $3.7\times10^{-8}cm^3$ ^{4}He(STP)/J (Ballentine & Burnard, 2002).

Radiogenic production of ^{3}He is ignored, as crustal production of ^{3}He is approximately eight orders of magnitude less than the production of ^{4}He (Ozima & Podosek, 2002). Radiogenic ^{4}He production is modeled only in the basement layer because crystalline basement materials typically have a much higher concentration of uranium and thorium (Parker, 1967) available for ^{4}He production. Therefore, the crystalline basement is assumed to be the largest contributor of radiogenic heat and helium.

In Section 3.3.2, we continue by combining the radiogenic heat and helium production with buoyancy-driven convection in the basement layer to analyze the combined effect on the distribution of heat and helium signals. Our simulations indicate that both radiogenic helium production and buoyancy-driven recirculation at depth, within a high-k basement that is capped by a low-k layer, can drastically impact near-surface helium ratios. Both deep processes cause decoupling of mantle/magmatic heat and helium signals near the surface.

3.3.1 Radiogenic heat and helium production in the basement.

The effect of radiogenic helium production in the basement on R/R_a values is shown in Figure 7c. The increased production of ^{4}He causes an expected decrease in R values. Unexpected is the increase in R/R_a values under the fracture in the basement layer. Further inspection shows that $[^4He]$ is decreased relative to $[^3He]$ in this region. The radiogenic

production causes an increase in the vertical gradient of ^{4}He concentration, allowing for higher upwards fluxes of the isotope out of the basement and into the fracture above.
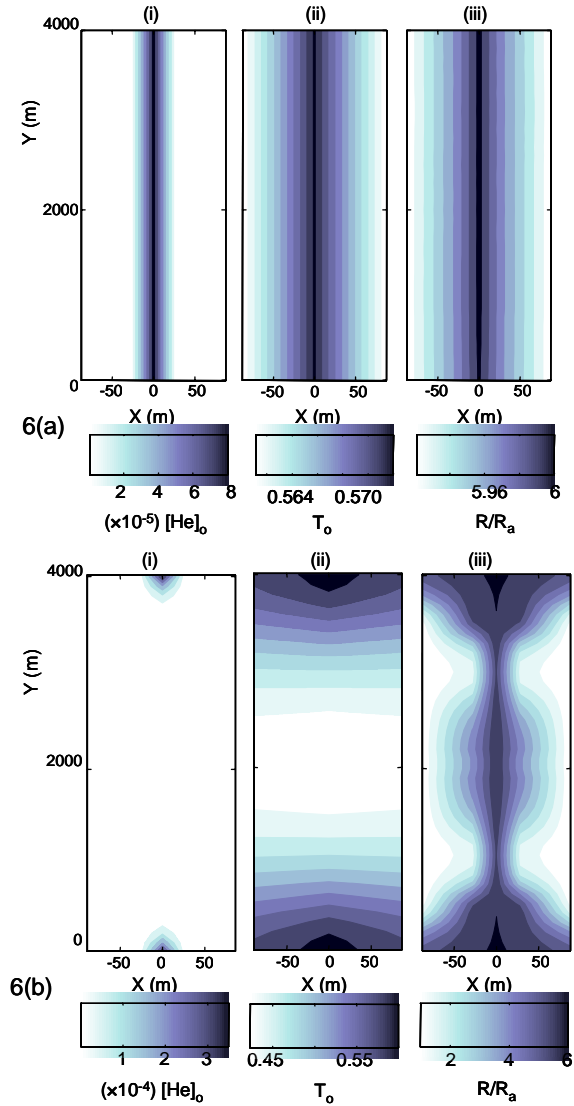

Figure 6.   *[He]$_o$ (i), T$_o$ (ii), and R/R$_a$ (iii) near the fracture at x=0m and z= -1050m for (a) coupled advective transport and (b) buoyancy-driven fracture convection. (a) All three signals have the same contour pattern, indicating that heat and helium transport is coupled. (b) Upwelling occurs at the sides of the fracture (y≈0m, y≈4000m). Even though downwelling occurs at the center (y≈4000m) and helium concentrations are comparatively low in this region, R values are elevated due to the high degree of mixing caused by the convective flow inside the fracture.*

3.3.2 Buoyancy-Driven Basement Convection

The presence of small circulation cells in the upper portion of the crystalline basement has been postulated to explain super-saline conditions found in waters originating from these depths (Aquilina et al., 2000; Clauser et al., 2002). Recirculation of deep waters can result in the enrichment of chemical species dissolved from the fractured and weathered bedrock. Thus, it may also be possible that enrichment of ^{4}He occurs by the same process.

To test this hypothesis, we increase the permeability of the basement material to 4×10^{-16} m^2, the same value as the overlying primary rock unit. To encapsulate convection within the basement, we impose a single confining layer (k=1×10^{-22}m^2) over the basement material. This arrangement is meant to represent higher permeability, weathered, and fractured upper bedrock overlain by a low permeability layer, such as a shale or otherwise effectively impermeable sedimentary unit, as suggested for example for the Rhine Graben by Aquilina et al. (2000). Our results are shown in Figure 7d.

Two recirculation cells develop in the basement layer, with upwelling occurring under the fracture (Figure 7d). The most significant result of the buoyancy-driven recirculation is that the basement waters are now well-mixed so that little of the R-anomaly from the previous simulation remains. As a result, the waters above the basement near the fracture also have a more consistent value of R.

4. DISCUSSION

The variation between coupling and decoupling of heat, helium concentrations, and R/R$_a$ ratios highlights the need to more precisely define what is meant by decoupling of heat and helium.

In the case of buoyancy-driven fracture convection (Section 3.2), heat and helium follow the same flow paths in the fracture such that elevated helium concentration and temperature coincide where upwelling occurs (Figures 5b-i, 6b). However, R/R$_a$ values (Figure 4) sometimes used to represent the percentage of mantle helium (e.g. Griesshaber et al., 1992) do not necessarily coincide with helium concentrations or temperatures (Figure 6b). The convection cells keep the fluids in the fracture relatively well-mixed, so that R/R$_a$ values remain consistent throughout. However, the convection also acts as a mechanism to extract heat and helium from the basement, so that helium concentrations and temperatures remain elevated at discharge areas.

Sometimes R/R$_a$ ratios are relied upon to determine the relative contribution of mantle or magmatic sources to the temperature field and the chemistry of subsurface fluids. If we considered only temperature and R values, we would determine that there is decoupling both in the fracture at the downwelling zone and in the primary rock.

However, in the fracture heat and helium transport are not decoupled. Transport paths are shared by both tracers.

In regard to the effect of radiogenic heat and helium production, we encounter a similar situation. Transport paths for heat and helium are the same, both being controlled by advection. However, the addition of radiogenic helium serves to dilute the mantle/magmatic helium signal (Figures 7c and 7d).

We therefore define two terms differentiating whether decoupling results strictly from varying transport mechanisms of heat and helium or from a combination of transport mechanisms and other interacting subsurface processes: *Transport decoupling* occurs when heat and helium transport paths are not synchronized, as in the diffusive-heat/advective-helium case of Section 3.1.2. *Signal decoupling* is defined as the presence of decoupled heat and helium isotope ratio signals (T and R/R$_a$), regardless of whether the transport paths coincide. Signal decoupling may represent "true" transport decoupling, but not necessarily so. Signal decoupling can also occur due to mixing, as in the case of buoyancy-driven fracture convection (Section 3.2), or due to dilution of mantle/magmatic helium signals through radiogenic production of ^{4}He.

5. CONCLUDING REMARKS

We have shown the result of varied permeabilities of the primary rock and fracture system in an extensional basin overlying a crystalline basement on the transport of heat and helium. Simulations of buoyancy-driven fracture convection show that this process can have a significant effect on near-surface heat and helium signals. The ability of convection cells to create chemically well-mixed waters is evidenced by the homogeneity of R values. Convection cells are also effective at removing heat and helium from the crystalline basement, resulting in elevated temperatures and helium concentrations at discharge areas. Further, in-situ production of heat and ^{4}He through radiogenic decay of uranium and thorium (even only in the basement far away from the Earth's surface) can play a significant role in the interpretation of near-surface heat and helium signals by effectively "diluting" the overall mantle/magmatic helium component. The occurrence of buoyancy-driven convection cells in the basement, together with radiogenic helium production, affects both deep and near-surface signals, by allowing for greater mixing and causing a more consistent distribution of R/R$_a$.

Furthermore, we suggest that there is a need for a more definitive vocabulary concerning coupled and decoupled heat and helium transport. We define true transport decoupling as the process by which movement of heat and helium is along divergent transport paths. We define signal decoupling as the
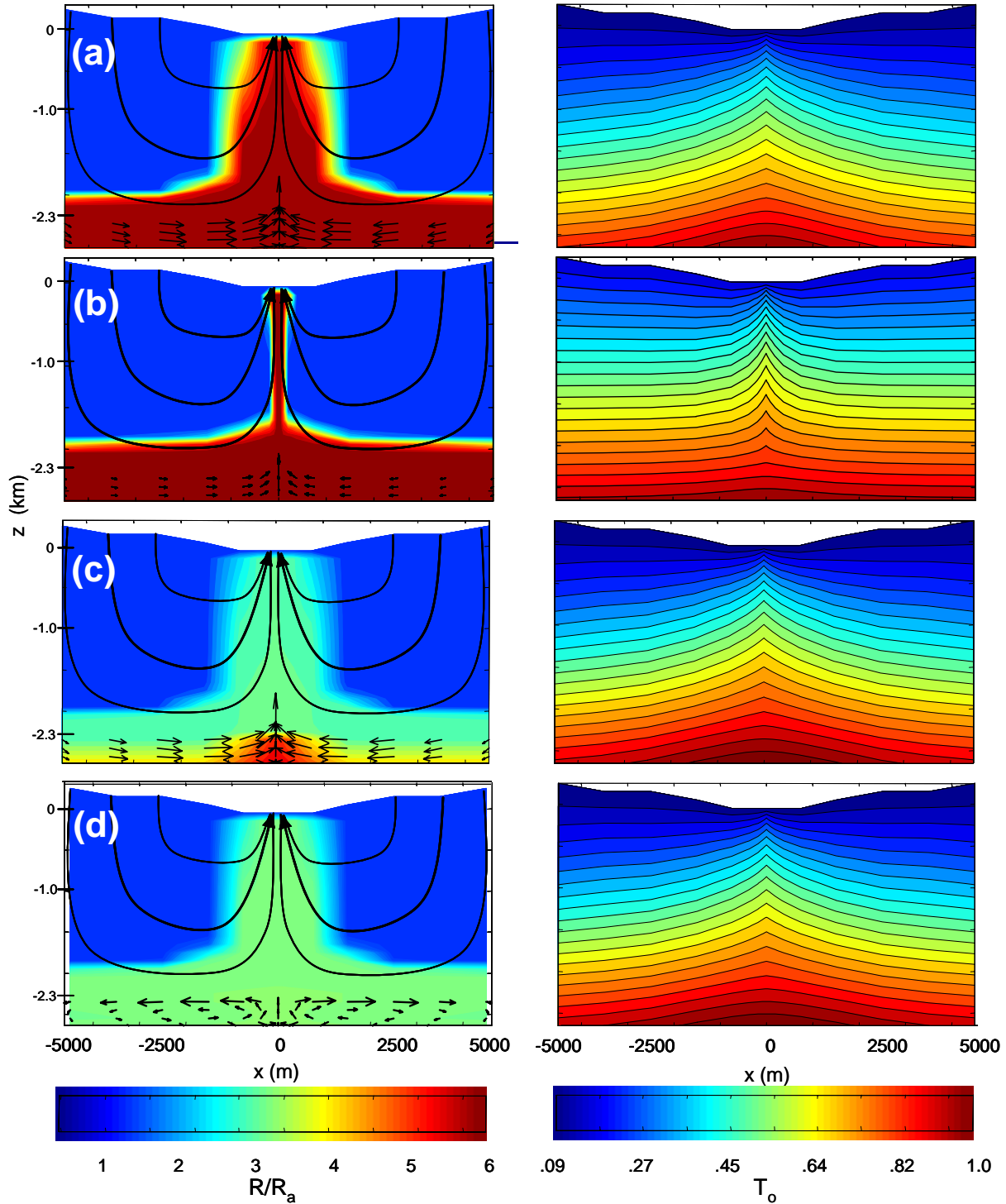
Figure 7. R/R$_a$ values (left column) and temperatures normalized to 110°C (right column). (a)Coupled advective transport (b) Buoyancy-driven fracture convection in a zone of upwelling (y=50m). (c) Coupled advective transport with radiogenic helium production in the basement. (d) Radiogenic helium production and buoyancy-driven basement convection. Arrows indicate direction of flow, lengths represent relative velocity (not to scale), streamlines are sketched. Although patterns and average values of R/R$_a$ are very different in each case, temperatures remain fairly constant. (c and d)Temperatures in the crystalline basement are somewhat elevated due to radiogenic heat production, but near-surface temperatures remain relatively unchanged. In contrast, near-surface helium ratios (R/R$_a$) are decreased by half the original value in this conservative estimate where radiogenic helium production occurs only within the crystalline basement.

phenomenon of decoupling of measured magmatic/mantle heat and helium, regardless of whether or not their transport paths coincide.

Since it may be impossible from the near-surface to discern whether a system is exhibiting transport or merely signal decoupling, our research highlights the need to use multiple data sets (temperature, helium concentration, radiogenic heat and helium production, groundwater recharge rates, etc.) to constrain the regime of fluid and heat flow in a geothermal reservoir. For example, detailed studies of aqueous chemistry can be beneficial in determining the source of fluids within a system. The disadvantage to this, however, is that such analyses depend on compatible tracers that are reacting with the surrounding rock on levels that are difficult to estimate. In contrast, noble gases may be used as incompatible tracers. For example, an analysis of all stable noble gases found in a water sample, as often done for general groundwater studies (e.g. Castro 1998a), and as proposed by Saar et al. (2005) for volcanic hydrologic systems can improve our understanding of the relative contributions of subsurface and atmospheric waters, their interactions, and related mass and energy (e.g., heat) transport processes.

REFERENCES

Aquilina L., A. Genter, P. Elsass, and D. Pribnow, Evolution of fluid circulation in the Rhine Graben: Constraints from the chemistry of present fluids, in Hydrogeology of Crystalline Rocks. I. Stober and K. Bucher (eds.), 177-203, Kluwer Acad., Norwell, Mass., 2000.

Bach, W., D. Naumann, J. Erzinger, A helium, argon, and nitrogen record of the upper continental crust (KTB drill holes, Oberpfalz, Germany): implications for crustal degassing. *Chem. Geol.* 160(1-2):81-101, 1999.

Bächler, D., T. Kohl, and L. Rybach, Impact of graben-parallel faults on hydrothermal convection— Rhine Graben case study. *Phys. Chem. Earth.* 28:431-441, 2003.

Ballentine, C.J. and P.G. Burnard, Production, Release and Transport of Noble Gases in the Continental Crust in *Noble Gases in Geochemistry and Cosmochemistry*, vol. 47, D. Porcelli, C.M. Ballentine, and R. Wieler (eds.), 481-538, 2002.

Bickle, M.J. and D. McKenzie, The transport of heat and matter by fluids during metamorphism. *Contrib. Mineral. Petrol.* 95:384-392, 1987.

Bredehoeft, J.D. and I.S. Papadopulos, Rates of Vertical Groundwater Movement Estimated from the Earth's Thermal Profile, *Water Resour. Res., 1*(2),325-328, 1965.

Castro, M.C. A. Jambon, G. de Marsily, P. Schlosser, Noble gases as natural tracers of water circulation in the Paris Basin 1. Measurements and discussion of their origin and mechanisms of vertical transport in the basin. *Water Resour. Res.* 34(10):2443-2466, 1998a.

Castro, M.C.; P. Goblet, E. Ledoux, S. Violette, G. de Marsily, Noble gases as natural tracers of water circulation in the Paris Basin 2. Calibration of a groundwater flow model using noble gas isotope data. *Water Resour. Res.* 34(10):2467-2483, 1998b.

Castro, M.C., D. Patriarche, P. Goblet, 2-D numerical simulations of groundwater flow, heat transfer, and ^{4}He transport—implications for the He terrestrial budget and the mantle helium-heat imbalance. *Earth Planet. Sci. Lett.* 237:893-910. doi:10.1016/j.espl.2005.06.037, 2005.

Clauser C., E. Griesshaber, H. Neugebauer, Decoupled thermal and mantle helium anomalies: Implications for the transport regime in continental rift zones. *J. Geophys. Res., 107*(B11), 2269, doi:10.1029/2001JB000675, 2002.

Clauser, C., and H. Villinger, Analysis of conductive and convective heat transfer in a sedimentary basin, demonstrated for the Rheingraben. *Geophys. J. Int.* 100:393-414, 1990.

Griesshaber, E., R.K. O'Nions, and E.R. Oxburgh, Helium and carbon isotope systematics in crustal fluids from the Eifel, the Rhine Graben and Black Forest, F.R.G. *Chem. Geol.* 99:213-235, 1992.

Hilton, D.R., The helium and carbon isotope systematics of a continental geothermal system: Results from monitoring studies at Long Valley Caldera (California, USA). *Chem. Geol.* 127(4):269-295, 1996.

Lopez, D.L. and L. Smith, Fluid flow in fault zones: Analysis of the interplay of convective circulation and topographically driven groundwater flow. *Water Resourc. Res.* 31(6):1489-1503, 1995.

Manning, C.E. and S.E. Ingebritsen, Permeability of the continental crust: implications of geothermal data and metamorphic systems. *Reviews of Geophysics, 37*(1), 127-150, 1999.

O'Nions, R.K. and E.R. Oxburgh, Heat and helium in the Earth. *Nature.* 306: 429-431, 1983.

Oxburgh, E.R., and R.K. O'Nions, Helium Loss, Tectonics, and the Terrestrial Heat Budget. *Science.* 237: 1583-1588, 1987.

Ozima, M. and F.A. Podosek, *Noble Gas Geochemistry.* 2nd ed. Cambridge UP: New York, 2002.

Parker, R.L., Composition of the Earth's crust, in *Data of Geochemistry*, 6th ed., *Prof. Pap. 440-D*, D1-D19, U.S. Geol. Surv., Reston, VA, 1967.

Pruess, K., *TOUGH2—A general purpose numerical simulator for multiphase fluid and heat flow*, Report LBNL-29400, Lawrence Berkeley National Laboratory, Berkeley, Calif., 1999.

Saar, M.O. and M. Manga, Depth dependence of permeability in the Oregon Cascades inferred from hydrogeologic, thermal, seismic, and magmatic modeling constraints, *J. Geophys. Res.*, *109*, B04204, doi:10.1029/2003JB002855, 2004.

Saar, M.O., M.C. Castro, C.M. Hall, M. Manga, and T.P. Rose, Quantifying magmatic, crustal, and atmospheric helium contributions to volcanic aquifers using all stable noble gases: Implications for magmatism and groundwater flow. *G-Cubed.* 6(3): doi:10.1029/2004GC000828, 2005.

Shan, C. and K. Pruess, *EOSN: A TOUGH2 Module for Noble Gases*, Report LBNL-52379, Lawrence Berkeley National Laboratory, Berkeley, Calif., 2003.

Smith, L. and D.S. Chapman, On the Thermal Effects of Groundwater Flow 1. Regional Scale Systems. *J.Geophys. Res.* 88(B1):593-608, 1983.

Stute, M., C. Sonntag, J. Deák, and P. Schlosser, Helium in deep circulating groundwater in the Great Hungarian Plain: Flow dynamics and crustal and mantle helium fluxes. *Geochim. Cosmochim. Acta.* 56:2051-2067, 1992.

Torgersen, T., Defining the role of magmatism in extensional tectonics: Helium-3 fluxes in extensional basins. *J. Geo. Res.* 98(B9):16,257-16,269, 1993.

Torgersen, T., S. Drenkard, K. Farley, P. Schlosser, and A. Shapiro, Mantle Helium in the Groundwater of the Mirror Lake Basin, New Hampshire, U.S.A., in *Noble Gas Geochemistry and Cosmochemistry.* J. Matsuda (ed.), 279-292, Terra Scientific Publishing Company, Tokyo, Japan, 1994.

Torgersen, T., S. Drenkard, M. Stute, P. Schlosser, and A. Shapiro, Mantle helium in ground water of eastern North America: Time and space constraints on sources. *Geology.* 23(8):675-678, 1995.

Zhao, X., T.L.B. Fritzel, H.A.M. Quinodoz, C.M. Bethke, and T. Torgersen, Controls on the distribution and isotopic composition of helium in deep ground-water flows. *Geology.* 26(4):291-294, 1998.